

University of Louisville

## ThinkIR: The University of Louisville's Institutional Repository

---

Electronic Theses and Dissertations

---

12-2021

### Computational modeling of 3D-printed Lactobacillus-antibiotic scaffolds for bacterial vaginosis.

Veeresh P. Rai  
*University of Louisville*

Follow this and additional works at: <https://ir.library.louisville.edu/etd>



Part of the [Biomedical Engineering and Bioengineering Commons](#)

---

#### Recommended Citation

Rai, Veeresh P., "Computational modeling of 3D-printed Lactobacillus-antibiotic scaffolds for bacterial vaginosis." (2021). *Electronic Theses and Dissertations*. Paper 3917.  
<https://doi.org/10.18297/etd/3917>

This Master's Thesis is brought to you for free and open access by ThinkIR: The University of Louisville's Institutional Repository. It has been accepted for inclusion in Electronic Theses and Dissertations by an authorized administrator of ThinkIR: The University of Louisville's Institutional Repository. This title appears here courtesy of the author, who has retained all other copyrights. For more information, please contact [thinkir@louisville.edu](mailto:thinkir@louisville.edu).

COMPUTATIONAL MODELING OF 3D-PRINTED, *LACTOBACILLUS*-ANTIBIOTIC  
SCAFFOLDS FOR BACTERIAL VAGINOSIS

By

Veeresh P. Rai  
B.S., University of Louisville, 2020

A Thesis  
Submitted to the Faculty of the  
University of Louisville  
J.B. Speed School of Engineering  
as Partial Fulfillment of the Requirements  
for the Professional Degree


MASTER OF ENGINEERING

Department of Bioengineering

December 2021



COMPUTATIONAL MODELING OF 3D-PRINTED *LACTOBACILLUS CRISPATUS*-  
ANTIBIOTIC SCAFFOLDS IN THE FEMALE REPRODUCTIVE TRACT

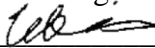
Submitted by:   
\_\_\_\_\_  
Veeresh P. Rai

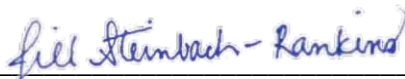
A Thesis Approved On


\_\_\_\_\_  
12/1/2021

(Date)

by the Following Reading and Examination Committee

  
\_\_\_\_\_  
Dr. Hermann B. Frieboes, Thesis Director

  
\_\_\_\_\_  
Dr. Jill M. Steinbach-Rankins

  
\_\_\_\_\_  
Dr. Nihat Altiparmak

## ACKNOWLEDGEMENTS

This project was made possible by the guidance of my thesis mentor, Dr. Hermann B. Frieboes. Additionally, the insights of the members of the Reading and Examination Committee, Dr. Jill M. Steinbach-Rankins and Dr. Nihat Altiparmak, were instrumental. An additional acknowledgement for Michael Halwes and Dylan Goodin, the first of which provided the foundational model for this project and the second of which whose aid was very beneficial to the overall success of the project.

## ABSTRACT

The standard treatment for bacterial vaginosis (BV) is currently antibiotics, such as metronidazole, clindamycin, or tinidazole. These antibiotics are highly effective in getting rid of bacteria in the female reproductive tract (FRT); however, there are some bacteria that provide benefits to the FRT which also get expunged. While there are many strains of bacteria that play a beneficial role in the FRT, *lactobacilli* are among the most important. These bacteria are responsible for maintaining a healthy environment in the FRT via pH regulation by lactic acid metabolism. Antibiotics eliminate all bacteria from an environment, including *lactobacilli*, and as a result, antibiotics are efficacious in the short run, but due to the lack of *lactobacilli*, recurrence of BV is possible. While recurrence is not guaranteed to occur as a result of the lack of *lactobacilli*, it certainly is common enough to warrant studies on recurrence prevention, as up to 50% of women with BV experience recurrence within 1 year of treatment <sup>[9]</sup>. The proposed solution is a tandem approach to BV treatment, involving an initial antibiotic treatment followed by probiotic *lactobacillus crispatus* (*L.cr.*) treatment; however, therein lie additional problems. Probiotics are still the topic of investigation for a variety of health issues, and as such have yet to be clinically proven for BV treatment. As such, in order to investigate probiotics in the context of BV more efficiently, a mathematical model was built to simulate *L.cr.* release and antibiotic release from 3D-printed scaffolds, as well as associated phenomena such as lactic acid production and pH change. The findings from this model conclude that the scaffold degradation rate bears the most impact on the time of release of antibiotic and probiotic from the scaffold, 1-2 days are required in between antibiotic and probiotic release to avoid any interaction between the two agents, and that

the release rate from the scaffold provides significant alterations in release kinetics provided that there is no overlap between antibiotic and probiotic release.

## TABLE OF CONTENTS

APPROVAL PAGE .....	ii
ACKNOWLEDGEMENTS .....	iii
ABSTRACT .....	iv
LIST OF TABLES .....	vii
LIST OF FIGURES .....	viii
1. INTRODUCTION .....	1
2. INSTRUMENTATION AND EQUIPMENT .....	4
3. PROCEDURE .....	5
4. RESULTS AND DISCUSSION OF RESULTS .....	26
5. CONCLUSIONS .....	32
6. RECOMMENDATIONS .....	34
REFERENCES .....	36



## LIST OF TABLES

Table 1: System Parameters.....	19
Table 2: System Variables .....	20

## LIST OF FIGURES

Figure 1: System Geometry .....	6
Figure 2: Time of Release vs. $k_D$ .....	29
Figure 3a-b: Probiotic Release Profile with varying time-delays due to varying $k_D$ .....	30
Figure 4a-d: Probiotic Release Profiles with Varying Release Rates .....	31
Figure 5a-d: Time to Reach Probiotic Release Amounts vs. Release Rate .....	32
Figure 6a-b: Lactic Acid Release with Associated pH Change over Time .....	33

## 1. Introduction

According to the Centers for Disease Control and Prevention, 29.2% of women in the United States between the age of 14 – 49 have bacterial vaginosis (BV) <sup>[1]</sup>. BV is a condition which occurs as a result of increased biodiversity in the female reproductive tract (FRT) due to an imbalance in the microbiota of the female reproductive tract. This results in an excess of anaerobes, the most prevalent of which is *Gardnerella vaginalis* (*G.v.*). Symptoms include itching, burning during urination, abnormal vaginal discharge, and foul-smelling vaginal odor <sup>[2]</sup>. The current standard of treatment for women with BV is prescribed oral or topical antibiotics to target *G.v.* and while antibiotics are effective in getting rid of *G.v.*, the antibiotics also deplete beneficial bacteria, namely *Lactobacillus Crispatus* (*L.cr.*). One of the roles of beneficial bacteria is to regulate pH by metabolizing glucose into lactic acid. BV occurs when these bacteria are overrun by *G.v.* and the pH balance is disrupted. Thus, when antibiotics are delivered, they target all bacteria, which results in efficacy against BV in the short run, but depletion of beneficial bacteria such as *L.cr.*, often leading to recurrence <sup>[9]</sup>. Recurrence occurs since, due to the antibiotics targeting both beneficial and pathogenic species, there are not sufficient beneficial bacteria present to restore the pH balance. While antibiotic treatment of BV does not always result in BV recurrence, it also does not provide any countermeasures to prevent recurrence from happening; the treatment approach for recurrent BV is reactive rather than proactive. Beneficial bacteria such as *L.cr.* can be employed as probiotic treatment for BV to achieve proactive prevention of BV recurrence. This is because when *L.cr.* creates lactic acid, the surrounding environment becomes more acidic and, as a result, is

more favorable for proliferation of beneficial strains like *L.cr.* In turn, this helps restore the balance of bacteria between *L.cr.* and *G.v.* since probiotics prefers lower pH environments (< 4.5) while *G.v.* prefers higher pH environments (> 4.5) <sup>[17] [16][20]</sup>. Therefore, the ideal treatment for BV would target *G.v.* and other pathogenic bacteria while simultaneously creating a favorable pH environment for *L.cr.* to proliferate. While probiotics can certainly be employed to prevent BV recurrence, there are limitations; for instance, in order to ensure treatment efficacy, probiotics would require frequent, if not daily applications by the user, which can cause challenges with regard to user adherence to the treatment. Instead, a mechanism for probiotic delivery that would only require users to apply the treatment a single time would be ideal.

A solution that has been proposed to meet this need is an electrospun fiber mesh probiotic delivery system for the sustained release of *L.cr.* to treat BV. These fibers consist of hydrophilic polyethylene oxide (PEO) to encapsulate the *L.cr.*, which then would be electrospun with hydrophobic poly (lactic-co-glycolic acid) (PLGA). While fibers offer a host of benefits such as biodegradability for sustained release <sup>[22]</sup>, the spinning procedure itself can be difficult to scale. 3D-printed scaffolds using probiotic bio-ink are an alternative solution to meet the same need that the PEO-PLGA fiber mesh does in a more modifiable package. Functionally, the scaffold and fiber mesh are similar since each allows release of *L.cr.* into the female reproductive tract (FRT) via degradation of the delivery vehicle <sup>[22]</sup>. Additionally, both the fiber mesh and scaffold release lactic acid to create an initial favorable, acidic environment for the *L.cr.*, albeit from different sources. In fibers, the initial lactic acid release is caused by the PLGA

composition of the fiber itself; whereas in scaffolds, bacteria that has been printed into a scaffold will begin to proliferate and metabolize surrounding nutrients to create lactic acid, which releases as the scaffold degrades. As these bacteria proliferate, the probiotics will exhibit chemotactic movement towards glucose in order to survive and proliferate. As the *L.cr.* consumes glucose, it creates lactic acid as a metabolic byproduct <sup>[12]</sup>, thereby creating a more acidic environment and creating a more favorable environment for further *L.cr.* proliferation and inhibition of proliferation of *G.v.* By restoring acidic conditions, recurrence of BV should be prevented since *G.v.* viability is hindered in acidic environments and *L.cr.* proliferation is favored.

The advantages of probiotic treatment over antibiotic treatment are clear, which begs the question as to why it has not yet been implemented. Probiotics are still the topic of many research projects to determine efficacy in initial treatment of BV and effectiveness in prevention of recurrence. Not to mention, efficacy in initial treatment of BV and prevention of BV recurrence could be different depending on the delivery vehicle: 3D-printed scaffold, electrospun fiber mesh, or other delivery means. In soluble co-cultures, *L.cr.* has been shown to provide protection against *G.v.* infection and has also been shown to outcompete and treat *G.v.* infection; all of which would indicate that probiotic treatment of BV in some fashion is by no means a stretch of the imagination. The viability of probiotic treatment for BV has further been confirmed by success of probiotic treatment for BV recurrence in clinical trials, such as that of lactin-v and others <sup>[33][34]</sup>. What remains to be answered though is how best to deliver these probiotics. This is a fairly significant task, since, not only are there multiple viable delivery means, but there

is also a myriad of factors associated with each delivery vehicle that alter probiotic effectiveness: electrospinning parameters, polymer materials, fiber architecture, morphology, amount of and distribution of the incorporated active agent (the probiotic in this case), affinity for water, porosity, viscosity, salt and protein concentrations, pH, system geometry etc. While 3D-printed scaffolds have seen use in soft tissue and cartilage engineering, delivery of anesthesia agents, and antiviral drug delivery via intravaginal rings (IVRs) for vaginal applications, specifically the use of such scaffolds for BV treatment has yet to be explored extensively. These 3D prints have shown promise in cartilage engineering and soft tissue engineering since the features of a print, such as geometry, print composition, viscosity, etc., can be precisely modified to fit a specific need, as was the case for the soft tissue engineering application in Chawla et al. [25], cartilage engineering application in You et al [26], or in IVR synthesis of Januszewicz et al. [35]; and can be modified even further via a scaffold's cross-linking conditions [25].

Since 3D-printed scaffolds for BV treatment is fairly new territory, it is not immediately apparent how to set scaffold design parameters or how to optimally test scaffolds, especially considering that laboratory resources such as time or funding are finite. Previously, mathematical models such as those described in Halwes et al. and Clark et al. [27] have been immensely helpful in identifying key parameters or predicting results of interest. Mathematical modeling serves as a useful tool in guiding research since it allows for the testing of multiple factors independently or codependently in an accurate and efficient fashion. More specifically, kinetic models enable simulation of microbial process and predictions for *in vitro* or *in vivo* implications. So, in order to

investigate the 3-D printed probiotic-loaded scaffold as a treatment option for BV, the existing model from Halwes et al <sup>[13]</sup> concerning modeling of the fiber mesh probiotic delivery system will be expanded upon, since the existing model provides a comprehensive foundation for the modeling of probiotic release from 3-D printed scaffolds. The nature of probiotic release is quite different from drug release, however, since the movement of the drug is modeled via simple diffusion while the movement of the probiotic is dependent on a variety of factors. The existing computational MATLAB model was adapted to fit release specifications of 3D-printed scaffolds, simulate probiotic release patterns, simulate pH change, and test a variety of factors related to probiotic efficacy and recurrence prevention. Such a model will be able to steer research on probiotic treatment for BV desirable features for a probiotic 3D-printed scaffold.

## **2. Instrumentation and Equipment**

The majority of modeling work was done within MATLAB R2020b, although the model can be run on any version of MATLAB since 2013, as MATLAB R2013a has also been used to run the model. Moreover, a device with minimum 16 gigabytes RAM is required to run the model; however, that amount of memory is only sufficient to sustain 240 hours of model runtime. If more simulation time is required, a device with more RAM would be required. The RAM limitation does not affect the model's ability to produce an accurate solution, however. If attempting to run the model past a device's RAM limitation (i.e., trying to simulate 500 hours on a device with 16 GB RAM, which would only allow 240 hours simulation), the model runs such that the maximum amount

of data is stored before running out of memory, and then the program is stopped. This means that the solution obtained from such a run will still be accurate but will not contain values past the RAM limitation. In other words, if one tries to simulate 500 hours on a device that only allows 240 hours of simulation, MATLAB will function as expected and accurately simulate the 240 hours, however once the program is out of memory, MATLAB will stop running the code and there will not be a solution present for the remaining 360 hours.

### **3. Procedure**

#### 3.1 Original Model

The existing model describes the release profile of an antiviral drug from a PEO-PLGA nanofiber mesh delivery vehicle, which serves as the foundation for modeling 3D-printed probiotic scaffolds. The original model sets the geometry, restraints, domain, and degradation kinetics that are used in the additions to the model.

##### 3.1.1 System Geometry

The geometry set by the original model represents a sample of fiber mesh placed over a layer of vaginal tissue, which is intended to mimic the *in vivo* environment of the FRT. The fiber mesh is in fluid, whose domain is computationally represented as a cylinder with radius 0.5 cm ( $r_F$ ) and thickness 0.5 cm ( $h_F$ ). The fibers, which are modeled as cylinders, are treated as uniform, neglecting any variance between fibers.



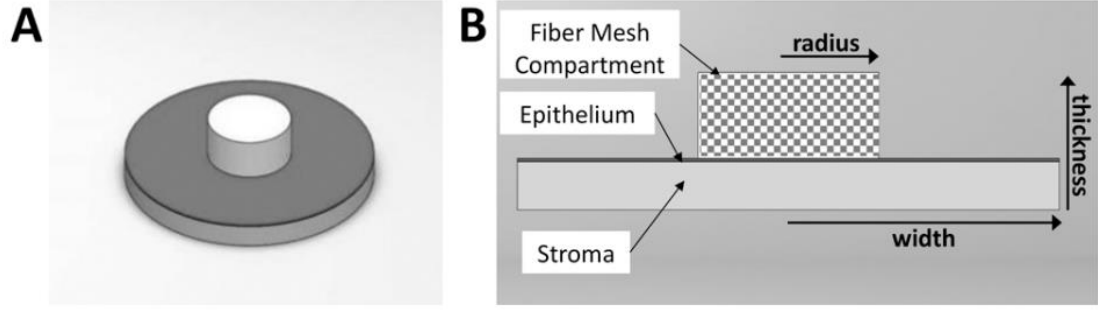


Figure 1: System geometry: (A) Isometric view of the system geometry, (B) system cross-section. The figure itself is from Halwes et al. <sup>[13]</sup>, since the geometry from the aforementioned study remained unchanged.

### 3.1.2 Fiber Degradation

Since PLGA can form polymer chains upwards of 10,000 repeating units, statistical moments were applied to polymer chains of length  $n > 9$ ,

$$\mu_k = \sum_{n=1}^{\infty} ((n)^k C_n)$$

(1)

where the  $k^{\text{th}}$  statistical moment depends on the degree of polymerization  $n$  and concentration of polymers of  $n$  chain length  $C_n$ . Thus,  $\mu_0$  is the concentration of polymer per unit volume,  $\mu_1$  is the concentration of monomers per unit volume, and  $\mu_2$  represents polymer polydispersity. From these three statistical moments, the polymer concentration change in time can be defined.

$$\frac{\partial C_M}{\partial t} = \frac{1}{r} \frac{\partial}{\partial r} \left( D_M r \frac{\partial C_M}{\partial r} \right) + 2k_d C_W (\mu_0 - C_M) \mu_0$$

(2a)

$$\frac{\partial C_n}{\partial t} = \frac{1}{r} \frac{\partial}{\partial r} \left( D_n r \frac{\partial C_n}{\partial r} \right) + 2k_d C_W \left( \mu_0 - \sum_{j=1}^n C_j \right) \mu_0 - (n-1)k_d C_W C_n \mu_0$$

$$2 \leq n \leq 9$$

(2b)

$C_M$  and  $C_W$  represent the concentration of polymer monomers and concentration of water, respectively, while  $r$  represents the cylinder radius,  $D_M$  and  $D_n$  represent the diffusion coefficients of monomer and polymer oligomer in water, and  $k_d$  is a kinetic rate constant for fiber degradation. Additionally, the diffusion of water into the polymer matrix can be modeled as follows:

$$\frac{\partial C_W}{\partial t} = \frac{1}{r} \frac{\partial}{\partial r} \left( D_W r \frac{\partial C_W}{\partial r} \right) - k_d C_W (\mu_1 - \mu_0) \mu_0$$

(3)

since PLGA is classified as a bulk erosion polymer.

Using the statistical moments, diffusion and degradation of polymers of chain length greater than 9 can be defined.

$$\frac{\partial \mu_0}{\partial t} = \sum_{j=1}^9 \frac{1}{r} \frac{\partial}{\partial r} \left( D_j r \frac{\partial C_j}{\partial r} \right) + k_d C_W (\mu_1 - \mu_0) \mu_0$$

(4a)

$$\frac{\partial \mu_1}{\partial t} = \sum_{j=1}^9 \frac{j}{r} \frac{\partial}{\partial r} \left( D_j r \frac{\partial C_j}{\partial r} \right)$$

(4b)

$$\frac{\partial \mu_2}{\partial t} = \sum_{j=1}^9 \frac{j^2}{r} \frac{\partial}{\partial r} \left( D_j r \frac{\partial C_j}{\partial r} \right) + \frac{k_d C_W \mu_0}{3} \left( \mu_1 - 2 \frac{\mu_2^2}{\mu_1} + \frac{\mu_2 \mu_1}{\mu_0} \right)$$

(4c)

Equations (2), (3), and (4) define polymer degradation and diffusion in the model and are relied on for drug and probiotic release.

### 3.1.3 Drug Release

In addition to utilizing fiber degradation from Halwes et al.<sup>[13]</sup>, the drug release from this model is adapted for an antibiotic.

$$\frac{\partial C_D}{\partial t} = \frac{1}{r} \frac{\partial}{\partial r} \left( D_{D,eff} r \frac{\partial C_D}{\partial r} \right) \quad (5)$$

The drug concentration  $C_D$  change in time depends on itself, the cylinder radius, and the effective diffusion coefficient of drug through the polymer matrix  $D_{D,eff}$ . This diffusion changes in time since as the fibers degrade, there is a decrease in hindrance to diffusion by the polymer chains, resulting in increased diffusivity.

$$D_{i,eff} = D_{i,eff}^0 \exp \left[ 2.5 \left( 1 - \frac{MW_n(t, r)}{MW_n(t = 0)} \right)^{0.5} \right] \quad (6)$$

$D_{i,eff}$  denotes the effective diffusion coefficient of a particular species: monomer, oligomer, water, or drug, while  $D_{i,eff}^0$  is the initial condition for each respective diffusion coefficient. Here,  $MW_n$  is calculated as

$$MW_n = \frac{\mu_1}{\mu_0} MW_{mon} \quad (7)$$

and is the number-averaged molecular weight, with  $MW_{mon}$  representing the molecular weight of the monomer.

### 3.1.4 Boundary Conditions

The final element from Halwes et al. to be incorporated is the definition of boundary conditions of which there are two boundaries considered: the center of the fiber ( $r = 0$ ) and its edge ( $r = R$ ). Since symmetry is assumed at the fiber center, this yields the following:

$$\left. \frac{\partial C_i}{\partial r} \right|_{r=0} = 0 \quad (8a)$$

$$\left. \frac{\partial D_i}{\partial r} \right|_{r=0} = 0 \quad (8b)$$

with  $C_i$  as the concentration of a species and  $D_i$  as its diffusion coefficient.

Since mass transfer occurs at the fiber edge and involves drug molecules, monomers, oligomers, water, and probiotics to the surrounding aqueous environment, the boundary condition is as follows:

$$-D_i(r = R) \left. \frac{\partial C_i}{\partial r} \right|_{r=R} = k_{C,i}^{ext} (C_{b,i} - C_i(r = R)) \quad (9)$$

Here,  $C_{b,i}$  is the concentration of a particular species in the exterior environment, which is assumed as 0 for the monomer, oligomer, and drug and  $0.055 \text{ mol cm}^{-3}$  for water. The assumption of 0 is based on the turnover of surrounding fluid in physiological systems, which resembles a sink condition. The Sherwood number is used to estimate the mass transfer coefficient  $k_{C,i}^{ext}$ . The Sherwood number is a dimensionless number utilized in mass transfer to find the ratio of convective mass transfer to diffusive mass transport. For fluid flow over a cylinder, the Sherwood number

$$Sh = 2 = \frac{2k_{C,i}^{ext} R}{D_{i,w}}$$

(10)

depends on the radius of the cylinder  $R$  and the diffusion coefficient of each species  $D_{i,w}$ .

### 3.2 Probiotic and Scaffold Adaptations

With the foundations for fiber degradation, drug release, and boundary conditions set, the model by Halwes et al. can be adapted to accommodate probiotic release and scaffold degradation, as well as other related, crucial components such as glucose concentration, lactic acid concentration, lactic acid dissociation, and pH.

#### 3.2.1 Scaffold Degradation

The model domain from Halwes et al.<sup>[13]</sup> is a sample of an electrospun polylactic-co-glycolic acid (PLGA) fiber mesh in fluid, which is placed over a layer of vaginal tissue. In the original model, the interior of a single fiber served as the model domain; whereas now, the model domain is the interior of a single scaffold. More specifically, the model describes the interior of a single 3D-printed scaffold as the delivery vehicle, with a porous exterior containing antibiotic, and a gelatin-alginate interior containing *L.cr.* Geometrically, the two delivery vehicles are similar, so from a modeling perspective, there are two functional differences to address. The first of these is the compartmental nature of the scaffold versus the fiber mesh. Scaffolds can be printed using a combination of inks, each with their own composition. Therefore, the interior of the scaffold can be printed with probiotics while the exterior is printed with the antibiotic. As the scaffold degrades from the exterior inwards, there is an initial release of antibiotic, followed by

release of probiotic. The compartmental nature of the scaffold is modeled by implementing a delay in the form of a unit step function on the release of the probiotic. The delay is based on the status of scaffold degradation; if and only if the scaffold has degraded to a user-defined amount, probiotic release occurs, shown below.

$$S = \begin{cases} 1, & \frac{\sum_{i=1}^9 C_i}{\mu_0} \geq T, T \in [0,1] \\ 0, & \text{otherwise} \end{cases} \quad (11)$$

$S$  represents the condition that determines whether or not there will be probiotic release,  $C_i$  represents the concentration of polymer chains of length 1 (monomer) to 9,  $\mu_0$  represents the total polymer concentration, and  $T$  represents the threshold at which release occurs, which is a value between 0 and 1.  $C_i$  is constantly updated in time so if the ratio of polymer constituents to total fiber concentration is greater than or equal to the user-defined threshold, 1 is set for the value of  $S$  and probiotic release occurs. Otherwise, the value for  $S$  is 0, and probiotic release does not occur.

The second functional difference between the fiber mesh and scaffold to address is the rate at which release occurs from each vehicle. Release is governed mainly by fiber geometry and fiber degradation rate. Worth noting is that the mechanism of degradation is not of interest in this model and so while there may be differences between the mechanisms of fiber degradation and scaffold degradation, we are only interested in the functional difference between the two. In other words, while the mechanism of scaffold degradation may be different from fiber degradation, the modeled fiber degradation can be adapted to reflect scaffold degradation. Worth mentioning is that pore sizes between the fiber and the various compartments of a scaffold are different depending on the

composition of each vehicle. However, since the same geometry is assumed between the scaffold and fiber, this extends to the pore sizes as well. Moreover, since the fiber mesh geometry is applied to the scaffold, the degradation rate of the fiber mesh is all that remains to be adjusted in order to accurately model a scaffold. Scaffolds tend to degrade more slowly than fibers<sup>[27]</sup>, so the degradation rate was calibrated to reflect this. The desired output for probiotic release was such that probiotic release would not coincide with a substantial concentration of antibiotic, so the degradation rate was calibrated accordingly. The degradation rate was calibrated to acquire delays of varying lengths; a narrow range of the degradation rate that would provide close to the desired delay was established via estimation, then linear regression was used to find the degradation rate value that corresponded to the desired delay.

### 3.2.2 Probiotic Release

The first addition to the existing system is the modeling of probiotics, which requires consideration of modeling live organisms as opposed to chemical compounds. Realistically, the probiotics do not release from the scaffold the same way a drug would; where a drug's behavior can be considered homogenous between spatial points, each probiotic is an individual organism that behaves slightly incongruously from another probiotic at a different spatial point, in addition to the fact that probiotics are much larger than an individual drug molecule, and probiotics also begin proliferating after release. In order to accurately model probiotic behavior, the live nature of the probiotic must be considered. The number of probiotics within a scaffold can be up to  $5 \times 10^7$  colony forming units (CFUs)<sup>[22]</sup>, so treating each of these as an individual organism would be

computationally strenuous. As such, the approach to modeling the probiotic requires the assumption that each individual probiotic can be treated as an aggregate organism and that any idiosyncratic behavior from the probiotics can be considered negligible overall.

With this assumption made, the nature of probiotic release must be considered. Unlike a drug, the movement of probiotics is not solely dependent on simple diffusion; there are chemotactic elements to examine with probiotics that are not present with a drug. Firstly, probiotics will exhibit chemotaxis towards glucose since this is the source of their nutrient which is required for proliferation as well as lactic acid production <sup>[15]</sup>. Since glucose allows for probiotic survival, chemotaxis towards glucose is a stronger influence on probiotic movement than simple diffusion <sup>[15]</sup>. As mentioned previously, probiotic consumption of glucose allows probiotics to produce lactic acid, which is another important factor for probiotic survival as well as the second chemotactic element of probiotic movement. The probiotics produce lactic acid thereby lowering the pH of the surrounding environment and helps create a more favorable environment for probiotic survival <sup>[12]</sup>. Therefore, chemotaxis towards lactic acid can be considered a stronger influence on probiotic movement than simple diffusion, but not as strong as chemotaxis towards glucose. The equations governing probiotic release incorporate glucose concentration, lactic acid concentration, antibiotic concentration, as well as scaffold degradation.

$$\frac{dC_p}{dt} = (k_p \cdot C_p - k_d \cdot C_p - (k_{AD} \cdot C_D + k_R \cdot (\mu_0 - \mu_{0,t})) \cdot C_p) \cdot S \quad (12)$$

$$k_p = k_{pmax} \cdot \left( \frac{C_G}{K_S + C_G} \right) \cdot \left( 1 - \frac{C_A}{C_{Amax}} \right)$$



The change in probiotic concentration ( $C_p$ ) over time is expressed in equation (12) while the growth rate of probiotics  $k_p$  is expressed in equation (13). First and foremost, all terms in the probiotic equation are multiplied by the unit step function  $S$ , which indicates that until there has been sufficient degradation of the polymer, there is no significant change in the probiotic behavior. When the unit step function is evaluated as 1, the probiotic concentration is dependent on itself, the probiotic death rate  $k_d$ , the death rate due to antibiotic interaction  $k_{AD}$ , the release rate of probiotic from the scaffolding  $k_R$ , the total polymer concentration  $\mu_0$  and  $\mu_{0,t}$ , and the unit step function  $S$ , as defined in equation (11). Probiotic growth cannot be treated as constant, since the growth is usually a function of the system's environment and time. Instead, probiotic growth  $k_p$  follows the Michaelis-Menten model of enzyme kinetics applied by Monod to microorganism growth<sup>[21]</sup>. The Monod model accounts only for the nutritional limitation of probiotic growth by glucose affinity; however, the contribution and inhibition of probiotic growth by probiotic lactic acid production must also be considered. The probiotic growth rate is always a fraction of  $k_{Pmax}$ , which is the maximum growth rate of the probiotic. The magnitude of this fraction is dependent on the glucose concentration  $C_G$ , the probiotic affinity for glucose or half-velocity constant  $K_S$ , the lactic acid concentration  $C_A$ , and the maximum lactic acid concentration  $C_{Amax}$ . Probiotic concentration, and by extension probiotic growth rate, will increase or decrease depending on how much glucose is available; high glucose will result in more proliferation while low glucose results in the opposite, which is accounted for by the Monod model. Probiotic proliferation rate also depends on lactic acid concentration since a primary function of probiotics in the FRT is to regulate pH, which is achieved by lactic acid production by probiotics. However,

probiotics will not proliferate as readily if there is already sufficient lactic acid in the environment, as the undissociated form of lactic acid is a main inhibitor of probiotic growth <sup>[5][11]</sup>. Undissociated lactic acid also serves as an indicator of the favorability of an environment for probiotics; once the concentration of lactic acid reaches its optimal point in the environment to host probiotics, the probiotics will maintain that concentration by either increasing or decreasing probiotic growth as needed. This relationship with lactic acid concentration can be expressed utilizing Briggs-Haldane kinetics (a derivation of the Michaelis-Menten model) <sup>[28][29]</sup> and is represented by the second parenthetical term in the probiotic growth rate equation.

Aside from  $k_P$ , the rest of the terms in the probiotic equation contribute to loss of the probiotic from different sources. The first loss term is  $k_d$ , which represents general death of probiotic and is assumed constant. This assumption is possible since fluctuations in death rate due to glucose or lactic acid concentration are already considered in the probiotic growth rate. While the death rate  $k_d$  does not change,  $k_P$  does change as the environment becomes more or less favorable for the probiotic which results in a relative change between the growth rate  $k_P$  and the death rate  $k_d$ . Bear in mind that the model domain only consists of a single scaffold, and while  $k_d$  accounts for some probiotic loss from the scaffold, there are two additional sources of probiotic loss: probiotic-antibiotic interaction and the release of probiotic from the scaffold, which are represented by  $k_{AD}$  and  $k_R$ , respectively. Since antibiotics used to treat BV do not selectively target bacteria, if there is any overlap between probiotic and antibiotic release, the antibiotics will immediately kill the probiotic. Additionally,  $k_R$  represents the rate at which bacteria are

released from the scaffold and move towards glucose as the scaffold degrades. The release rate  $k_R$  is multiplied by the term  $\mu_0 - \mu_{0,t}$  which decreases the release rate as the scaffold degrades. More specifically,  $\mu_{0,t}$  is the polymer concentration at the first point where the ratio of oligomers of chain length 1 – 9 to the total polymer concentration is greater than or equal to the user-defined threshold; or, more simply put, it is the polymer concentration at the first point at which the unit step function  $S$  is equal to 1. In order to determine the value for  $\mu_{0,t}$ , the model must be ran to the point at which  $S$  is equal to 1; however, while this is feasible, it is not ideal to retroactively implement values for parameters. Therefore, until the value for  $\mu_{0,t}$  is known, it is initialized to 0. Then once the condition for  $S$  has been met, the value for  $\mu_{0,t}$  is updated. The effect that this has on the release rate  $k_R$  is that once the condition has been met,  $\mu_0$  increases as the scaffold degrades while  $\mu_{0,t}$  remains constant. This causes an increase in the release rate  $k_R$  due to the fact that as more of the scaffold has degraded away, the more readily and easily the probiotics can exit the scaffold.

### 3.2.3 Glucose and Lactic Acid Modeling

Glucose and lactic acid are crucial components of probiotic proliferation and survival, so the model would not be complete without their consideration. Note that diffusion has not been considered for glucose or lactic acid since the scaffold has a porous surface. This allows for an equilibrium to be assumed between the scaffold and the surrounding environment.

$$\frac{dC_G}{dt} = G_G - L_G C_G - k_G C_P + f_G$$

( 14 )

$$\frac{dC_A}{dt} = (G_A - L_A C_A + k_A C_P + f_A) + (k_r \cdot \ell \cdot a - k_f \cdot C_A) \quad (15)$$

The glucose equation and the first parenthetical term in the lactic acid equation follow the same format. Each equation has a gain term  $G$ , loss rate due to leakage  $L$ , forcing function  $f$ , and probiotic-related rate  $k$ . The gain term  $G$  represents entrance of the substrate into the system from the environment, while the subscripts  $G$  and  $A$  denote glucose and lactic acid, respectively. The rates  $k_G$  and  $k_A$

$$k_A, k_G \propto k_P \quad (16)$$

$$k_G = \frac{k_P}{Y_{P/G}} \quad (16a)$$

$$k_A = \frac{k_G}{Y_{A/G}} \quad (16b)$$

represent probiotic consumption of glucose and probiotic production of lactic acid and are proportional to the probiotic growth rate. The glucose consumption and lactic acid production rates are not constant during glucose fermentation since these rates are affected by rate of probiotic growth and substrate consumption <sup>[19]</sup>. The glucose consumption rate is dependent on probiotic growth  $k_P$  and a constant  $Y_{P/G}$  probiotic growth yield from glucose. The probiotic production rate of lactic acid is dependent on  $k_G$  and a constant  $Y_{A/G}$  which represents the lactic acid yield from glucose metabolism. Additionally,  $f_G$  and  $f_A$  are forcing functions for glucose and lactic acid which help restore or maintain steady-state conditions of each substrate. The lactic acid forcing function  $f_A$  represents lactic acid released from the PLGA-PEO fiber mesh, however this is negligible

when compared to the lactic acid production by probiotics. Moreover, the glucose forcing function  $f_G$  is also set to 0 since the other terms already maintain an equilibrium. The forcing functions were essentially infrastructure from the original model that were not needed for the new equations.

### 3.2.4 Lactic Acid Dissociation

The lactic acid equation also contains reaction kinetics from its dissociation that contribute to the overall lactic acid concentration. The dissociation's contribution to overall lactic acid concentration is represented by the second set of terms in equation (5). Moreover, the dissociation of lactic acid is necessary in order to measure pH and gauge the effect of probiotics. Lactic acid,  $C_3H_6O_3$ , dissociates into a lactate ion and hydrogen ion with forward and reverse rates  $k_f$  and  $k_r$ .



$$K_A = \frac{k_f}{k_r} \quad (15b)$$

$$k_r = \frac{k_f}{K_A} \quad (15c)$$

The forward and reverse rates were determined from the equilibrium constant of lactic acid dissociation  $K_A$ , which is equal to  $1.38 \times 10^{-4}$ . From here,  $k_f$  was estimated and the corresponding  $k_r$  was calculated. From the lactic acid dissociation, equations governing the dissociation equilibrium can be formulated,

$$\frac{dC_A}{dt} = k_r \cdot \ell \cdot a - k_f \cdot C_A$$

( 15d )

$$\frac{da}{dt} = k_f \cdot C_A - k_r \cdot \ell \cdot a$$

( 15e )

$$\frac{d\ell}{dt} = k_f \cdot C_A - k_r \cdot \ell \cdot a$$

( 15f )

where  $C_A$  represents the lactic acid concentration,  $\ell$  represents the lactate ion concentration, and  $a$  represents the acidic hydrogen ion concentration, all expressed in mol/mm<sup>3</sup>. The equations for lactate ion and H<sup>+</sup> follow the same kinetics, however they differ in their initial conditions which results in similar trends in their behavior but ultimately different equilibrium values.

### 3.2.5 pH Calculation

Since the H<sup>+</sup> ion concentration,  $a$ , is initially expressed in mol/mm<sup>3</sup>, a unit conversion is required to accurately calculate pH, since the pH equation requires a concentration expressed in molarity.

$$pH = -\log_{10}(a \cdot 10^6)$$

( 17 )

Here, 10<sup>6</sup> serves as the conversion factor from mol/mm<sup>3</sup> to mol/L, and hence molarity.

Table 1: System Parameters

Parameter	Definition	Value (Range)	Source
$k_d$	General probiotic death rate	$2.473 \times 10^{-3} \text{ h}^{-1}$ ( $2.47 \times 10^{-3}$ to $2.476 \times 10^{-3} \text{ h}^{-1}$ )	Calibrated
$k_D$	Degradation rate constant	$6.79 \times 10^{-2} \text{ h}^{-1}$ (0.44 to $1.9 \text{ h}^{-1}$ )	Calibrated

$k_{Pmax}$	Maximum probiotic growth rate	$1 \text{ h}^{-1}$ ( $0.95$ to $1.03 \text{ h}^{-1}$ )	Literature [24], calibrated
$k_{AD}$	Probiotic death rate due to antibiotic interaction	$1.25 \times 10^2 \text{ h}^{-1}$ ( $1.0 \times 10^2$ to $1.0 \times 10^3 \text{ h}^{-1}$ )	Calibrated
$k_R$	Release rate of probiotic from scaffold	$5 \times 10^{-1} \text{ h}^{-1}$ ( $5 \times 10^{-2}$ to $1 \text{ h}^{-1}$ )	Calibrated
$K_S$	Half-velocity constant for probiotics and glucose	$2 \times 10^{-1} \text{ mol/mm}^3$ ( $1.95 \times 10^{-1}$ to $2.05 \times 10^{-1} \text{ mol/mm}^3$ )	Literature [24], calibrated
$C_{Amax}$	Maximum lactic acid concentration	$6.03 \times 10^{-5} \text{ mol/mm}^3$ ( $5.0 \times 10^{-5}$ to $7.12 \times 10^{-5} \text{ mol/mm}^3$ )	Literature [30], calibrated
$G_G$	Glucose gain	$1 \times 10^{-4} \text{ mol}/(\text{mm}^3 \cdot \text{h})$ ( $1.0 \times 10^{-5}$ to $1.1 \times 10^{-4} \text{ mol}/(\text{mm}^3 \cdot \text{h})$ )	Calibrated
$G_A$	Lactic Acid gain	$6 \times 10^{-7} \text{ mol}/(\text{mm}^3 \cdot \text{h})$ ( $5 \times 10^{-7}$ to $7 \times 10^{-7} \text{ mol}/(\text{mm}^3 \cdot \text{h})$ )	Calibrated
$L_G$	Loss rate of glucose due to leakage	$1 \times 10^{-1} \text{ h}^{-1}$ ( $6.0 \times 10^{-2}$ to $1.023 \times 10^{-1} \text{ h}^{-1}$ )	Calibrated
$L_A$	Loss rate of lactic acid due to leakage	$2 \times 10^{-2} \text{ h}^{-1}$ ( $1.1 \times 10^{-2}$ to $2.08 \times 10^{-2} \text{ h}^{-1}$ )	Calibrated
$Y_{P/G}$	Yield of probiotic growth from glucose consumption	$1 \times 10^1$ ( $2.0$ to $5.0 \times 10^1$ )	Calibrated
$Y_{A/G}$	Yield of lactic acid from glucose consumption	1.8	Literature [31]
$K_A$	Lactic acid dissociation equilibrium constant	$1.38 \times 10^{-4}$	Literature [23]
$k_f$	Forward rate of lactic acid dissociation	$1.38 \times 10^{-9} \text{ mol/L}$ ( $1.38 \times 10^{-11}$ to $1.38 \times 10^{-7} \text{ mol/L}$ )	Calibrated

All rates are multiplied by the units of concentration in the model,  $\text{mol/mm}^3$ , which ultimately yields units of concentration per time,  $\text{mol}/(\text{mm}^3 \cdot \text{h})$ .

Table 2: System Variables

Variable	Definition
$C_i$	Polymer oligomer concentration for $i = 1, 2, \dots, 9$
$\mu_0$	Concentration of polymer per unit volume

$\mu_{0,t}$	Concentration of polymer per unit volume at first timepoint where $S = 1$
$k_P$	Probiotic growth rate
$C_G$	Concentration of glucose
$C_A$	Concentration of lactic acid
$k_G$	Probiotic consumption rate of glucose
$k_A$	Probiotic production rate of lactic acid
$k_r$	Reverse rate of lactic acid dissociation
$\ell$	Lactate ion concentration
$a$	$H^+$ ion concentration
$k_D$	Degradation rate constant of fiber
$T$	Scaffold degradation threshold that must be met before probiotics release

### 3.2.6 Parameter Calibration

Several system parameters were calibrated to their current value, as opposed to being obtained via literature or calculation. This calibration process was based on system stability, system efficiency, biological relevance, and literature. Whenever possible, literature values were used to obtain an initial value for a parameter, around which a range of values could be found. The range for literature values was established by mainly considering system stability and efficiency. For system stability and efficiency, the calibration of parameters was fairly consistent; if a value for a given parameter causes the system to be unable to converge to a solution or if said value causes erratic or nonsensical system behavior, that parameter value would not be included in the range. An example of erratic system behavior would be if a given parameter value results in an irregular waveform, whereas an example of nonsensical system behavior would be negative values for a system variable for which negative values are realistically impossible within the system, such as probiotic concentration, glucose concentration, lactic acid concentration, etc. System stability and efficiency were considered for all parameters, however there



were some parameters for which system stability and efficiency were the only considerations for calibration since they would typically have small ranges of values for which the system could converge to a solution and would have little change in system behavior across the range of values for which a solution was obtained. These parameters were  $G_G$ ,  $G_A$ , and  $Y_{P/G}$ .

While the approach to calibration with respect to system stability and efficiency was fairly uniform across system parameters, calibration with respect to biological relevance was more varied depending on the system parameter. For instance, the general probiotic death rate  $k_d$  was calibrated such that probiotic growth would not outpace probiotic death, resulting in the scaffold serving as an endless well of bacteria. If the death rate was too low, growth would occur uncontested and unfettered; however, if the death rate was too high, probiotics would simply die in the scaffold as opposed to being released. The calibration of the maximum probiotic growth rate  $k_{Pmax}$  followed a similar approach; if the maximum growth rate was too high, unrestrained growth would occur, while if it was too low, probiotic death would be dominant at equilibrium.

The scaffold degradation rate  $k_D$  was calibrated based on the desired delay. This was adapted from Halwes et al.<sup>[13]</sup> and varied to determine the relationship between  $k_D$  and corresponding delay. Once this relationship was established, the degradation rate was calibrated to find various lengths of delay.

The probiotic death rate due to antibiotic interaction  $k_{AD}$  was calibrated such that if there was significant overlap between antibiotic and probiotic release, this death rate would cause the probiotic concentration to be quickly exterminated by the antibiotic. Making this rate too low would correspond to the antibiotic causing an insufficient amount of probiotic death; however, making this rate too high would result in the probiotic dying off if there is any presence of antibiotic, regardless of concentration. Both of these phenomena would not be realistic since antibiotics in sufficient concentration will kill off any bacteria, but if 99% of the antibiotic has already released into the FRT, the remaining 1% of antibiotic would not be sufficient to eliminate all probiotics from the scaffold.

The release rate  $k_R$  was calibrated such that decay due to  $k_R$  would be distinguishable from decay due to  $k_{AD}$ , the probiotic death rate due to antibiotic interaction. As such,  $k_R$  would need to be sufficiently low in order to produce a pronounced decay curve, while  $k_{AD}$  would produce a decay curve that is immediate. A range of values was obtained based on the need to be able to attribute the cause of decay to either probiotic interaction with antibiotic or release from the scaffold. At the higher end of this range, it is more difficult to discern this, while it is easier at the lower end of the range. This is because a higher release rate yields more rapid probiotic decay, while a lower release rate yields a more pronounced decay. If the release rate is set sufficiently high, it is not possible to visually determine whether probiotic decay is occurring due to interaction with the antibiotic or due to the exit of probiotic from the scaffold. If, however, the release rate is set sufficiently low, this distinction is easier to make since a

pronounced decay would be caused by the release rate while a rapid decay would be caused by antibiotic interaction.

The calibration for the loss rate of glucose and lactic acid due to leakage  $L_G$  and  $L_A$ , respectively, utilized a similar approach, although the end goals for calibration of these terms were different. For glucose, the expectation is that there is sufficient glucose for the probiotics such that competition for nutrients does not factor into the probiotic concentration equilibrium. This is due to the fact that the scaffold itself is porous to the exterior environment and as the concentration of glucose inside the scaffold decreases, it is replenished by the entrance of glucose from outside the scaffold. Additionally, competition for glucose was not considered since only *L.cr.* was modeled; the presence of other bacteria was not considered due to the model domain consisting solely of the interior of a scaffold. With these considerations, the loss rate of glucose due to leakage could not be too high that it would result in system failure but could not be so low that the glucose concentration would decrease to 0 inside the scaffold. The loss rate of lactic acid due to leakage  $L_A$  was calibrated in a similar fashion; however lactic acid is expected to be released from the scaffold, unlike glucose. This is because the environment in which a scaffold is deployed would be the environment of a BV infection where pH is high and lactic acid concentration is low. As such, lactic acid from inside the scaffold would be expected to release into the environment after being produced by the probiotics in the scaffold. This is reflected in the calibration of  $L_A$  since making this rate too low would cause lactic acid to be produced unrestricted inside the scaffold, and it would make

the scaffold an endless well of lactic acid, while making the rate too high would result in system instability.

### 3.3 Verification

The model results were verified via analytical confirmation. The model was run and stopped at a random point where manual calculations for system variables at this point were made in Excel and compared to model calculations for the same variables. Upon assessment, the manual calculations were the same as the model calculations, with slight discrepancies due to floating point approximation in Excel. Since MATLAB and Excel can only be so precise in terms of storing values for floating point numbers, there were slight differences between manual and model calculations, but these differences were on orders of magnitude smaller than the precision of both MATLAB and Excel. In the model, the variables were stored with up to 15 digits of precision and Excel uses 15 digits of precision by default <sup>[36][37][38]</sup>. The maximum difference between manual and model calculations was  $1.08 \times 10^{-18}$  which is on an order of magnitude beyond the precision of MATLAB and Excel, which confirms that floating point approximation as the cause for this difference since there were no recorded differences within the precision of MATLAB or Excel. This method of analytical confirmation was possible since the model calculations are not stochastic; hence, if the calculations are correct at one point in the model, they are correct at any other point in the model since the calculations are rigid in terms of how they are made.

### 3.4 Validation

Currently, the modeling results are theoretical and as such have not yet been experimentally validated. Nonetheless, steps are in place for model validation; the first of which is to validate the scaffold degradation timeline. This would be done in 3 parts: (1) determining the scaffold degradation timeline for a scaffold printed with only *L.cr.*, (2) determining the scaffold degradation timeline for a scaffold printed with only antibiotic, and (3) determining the scaffold degradation timeline for a scaffold printed with both *L.cr.* and antibiotic. Blank scaffolds (scaffolds without bacteria) would also be printed to serve as a comparison for how bacteria affect scaffold degradation. These three parts would establish baseline expectations for how long a scaffold would degrade and how each agent (*L.cr.* and antibiotic) affects degradation. To do this, scaffolds would be printed with bioinks of various compositions, as specified earlier, then placed in simulated vaginal fluid<sup>[32]</sup> (SVF) in a 37°C environment, such as an incubator. These scaffolds would be assessed daily for structural integrity to determine exactly how long it takes for the scaffold to degrade entirely. Then, the timeline for degradation of the scaffolds can be implemented more precisely in the model.

The next step for validation would involve validating the probiotic release and associated effects of the probiotic on the surrounding environment. Validating probiotic release, at least as it has been presented in the model, is not straightforward. This is due to the nature of release from scaffolds itself; when a probiotic-loaded scaffold is delivered into an aqueous environment, the scaffold will eventually release some initial amount of CFUs of the probiotic, in this case *L.cr.* When this occurs, the CFUs that have been released eventually begin proliferating on their own, while the scaffold is

simultaneously releasing additional CFUs of *L.cr.* Release from a scaffold can be measured, however it is not feasible to distinguish the probiotics that have released from the scaffold itself and the probiotics that have grown as a result of a prior CFU being released from the scaffold and proliferating. The model domain consists of the interior of a scaffold, and as a result, proliferation of probiotic on the exterior of the scaffold, be it from released or surface-bound *L.cr.*, is not considered in any probiotic release curves. In other words, since the *in vitro* release of probiotics from a scaffold cannot be separated from the proliferation that occurs as a result of said release, it is not currently possible to validate the modeled probiotic release. This is because the model domain only consists of the interior of a scaffold, and as a result, only release is modeled, not proliferation. With that said though, other probiotic-related phenomena can still be validated; namely, the pH change. This can be done simultaneously with validating the scaffold degradation timeline. For scaffold degradation validation, probiotic-only, antibiotic-only, and probiotic-antibiotic scaffolds would be printed and placed in SVF and assessed daily for structural integrity. Additional assessments can be made to determine pH change; the initial pH of SVF would be measured, then pH would be measured at various timepoints. The timepoints of interest would likely be 1-hour, 4-hour, then daily for at least 10 days. These timepoints would help establish the rate by which probiotics cause surrounding pH to change, which can be incorporated into the model. Note that this would also provide validation for the Briggs-Haldane basis of probiotic growth modeling, which treats lactic acid as an inhibitor of probiotic growth. Since lactic acid is the primary determinant of pH<sup>[5][11]</sup> in the FRT, pH can be treated as a proxy for lactic acid, as undissociated lactic acid increases pH, and the dissociation of lactic acid causes decreased pH. If the pH

decreases to a particular point and then remains at that level, it would suggest that pH and lactic acid provide some inhibitory effect on probiotic growth, thereby validating the modeling approach to probiotic growth.

## **4. Results and Discussion of Results**

### 4.1 Release of Probiotic

In order for probiotics to affect their surrounding environment, they must be released such that they do not interact with the antibiotic; otherwise, they will be killed by the antibiotic and will exert negligible effect on the restoration of vaginal health. The most efficient way to delay this release is by altering the scaffold degradation rate  $k_d$ , since release occurs as a function of scaffold degradation. Hence, the relationship between the degradation rate and time of release was determined.

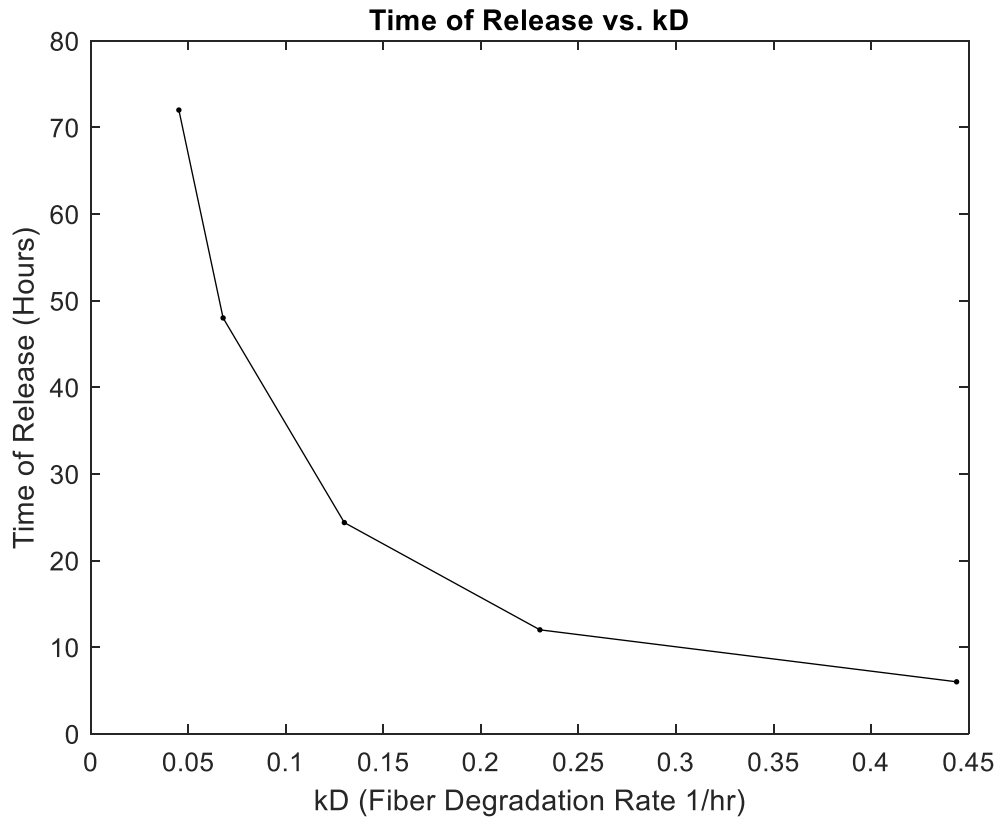


Figure 2: Time of Release vs.  $k_D$ . As fiber degradation rate increases, the corresponding delay of time of probiotic release is shortened. The points from left to right correspond to (0.05, 72), (0.07, 48), (0.13, 24), (0.23, 12), and (0.44, 6).

The relationship between  $k_D$  and corresponding time of release appears to follow a negative logarithmic curve where, as  $k_D$  is increased further and further, the time of release is delayed further, albeit to a lesser and lesser extent. To utilize this insight, a variety of probiotic release profiles were obtained, all of which had varying degradation rates which equated to different lengths of delays: 6-hour, 12-hour, 1-day, 2-day, and 3-day. The drug release from the model reaches 100% drug released in approximately 1.5 days, which means a delay of probiotic release by two days would avoid any interaction with the antibiotic.



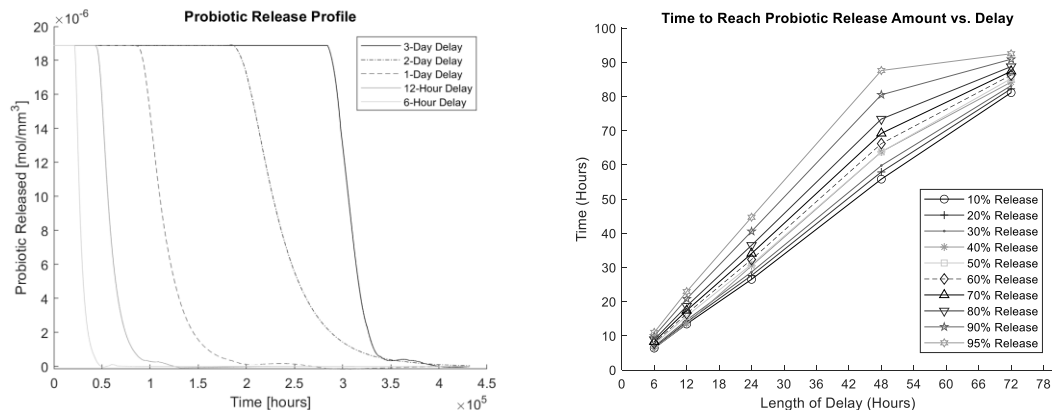


Figure 3a-b: (a) Probiotic Release Profile with varying time-delays as a result of varying scaffold degradation rate: 6-hour delay, 12-hour delay, 1-day delay, 2-day delay, and 3-day delay. (b) Time to reach various probiotic release checkpoints (25%, 50%, 75%, and 95%) vs. corresponding delay in hours (72, 48, 24, 12, 6). The green diamonds represent 25% probiotic release, the blue circles represent 50% probiotic release, the red squares represent 75% probiotic release, and the yellow triangles represent 95% probiotic release. The  $R^2$  correlation coefficient for each set of data was above 0.9.

Based on the release profiles from the model, delays of less than 1 day on the probiotic release are susceptible to antibiotic interaction, so a delay of at least 1 day would be required between antibiotic and probiotic release to ensure probiotic efficacy. This also indicates that the drug concentration at the 1-day mark is not sufficient to cause significant loss of the probiotic due to antibiotic interaction. These delays were achieved by adjusting the degradation rate  $k_D$ ; thus, an increase in degradation rate translates to faster release and a shorter delay of probiotic release.

The probiotic release can also be assessed by the time at which it reaches various probiotic release checkpoints (10%, 20%, 30%, 40%, 50%, 60%, 70%, 80%, 90%, and 95% release) compared to the associated delay. This relationship appears to be linear in nature, which indicates that a delay to probiotic release does not change the nature of the release itself; instead, it acts as a shift to the release. Upon linear regression, the  $R^2$  correlation coefficient was greater than 0.9 for each release amount, which further

suggests a linear relationship between time to reach a given probiotic release checkpoint and the corresponding delay.

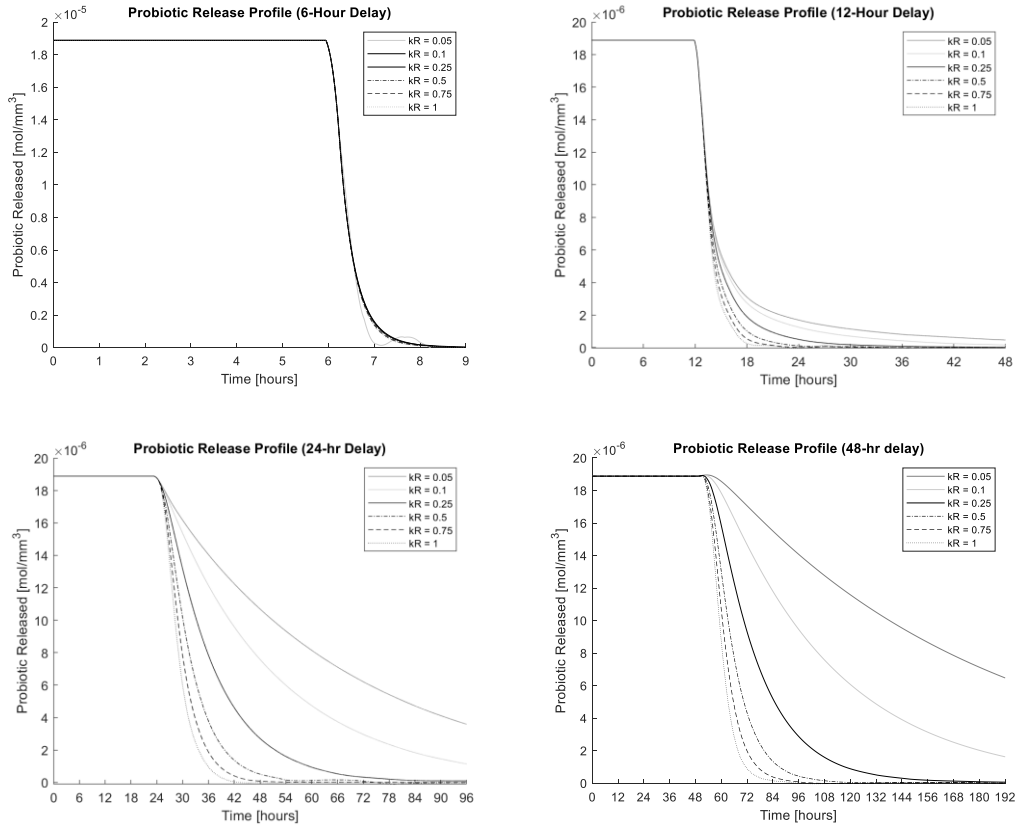


Figure 4a-d: Probiotic Release Profiles with varying release rates. (a) Top left panel: Probiotic release profile with 6-hour delay. (b) Top right panel: Probiotic release profile with 12-hour delay. (c) Bottom left panel: Probiotic release profile with 24-hour delay. (d) Probiotic release profile with 48-hour delay. The release rates  $k_R$  are as specified in the legend, ranging from  $5 \times 10^{-2}$  at the lowest,  $5 \times 10^{-1}$  at an intermediate level for  $k_R$ , and 1 at the highest.

Furthermore, altering release rate also shows impact on the probiotic release profile.

As the release rate  $k_R$  decreases, the probiotics are expected to take a longer time to exit the scaffold which is showcased in Figure 3.

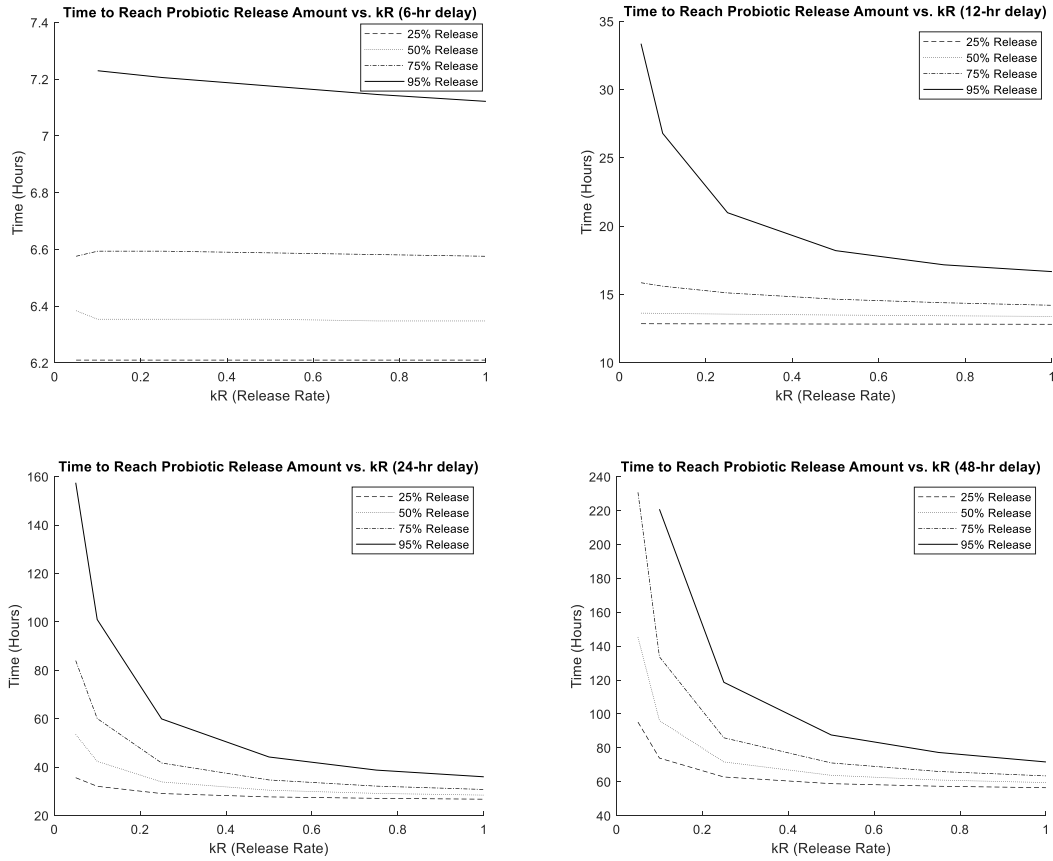


Figure 5a-d: Time to reach various probiotic release amounts (25%, 50%, 75%, and 95%) vs. corresponding release rate  $k_R$ . (a) Top left panel: Release checkpoint vs.  $k_R$  with 6-hour delay. (b) Top right panel: Release checkpoint vs.  $k_R$  with 12-hour delay. (c) Bottom left panel: Release checkpoint vs.  $k_R$  with 24-hour delay. (d) Top left panel: Release checkpoint vs.  $k_R$  with 48-hour delay.

It is important for the release rate to be distinguishable from the probiotic death due to antibiotic death rate  $k_{AD}$  since if the release rate is too high, it is difficult to attribute the cause of rapid decay to either a high release rate or probiotic interaction with antibiotic. For 1- and 2-day delays, the time to reach a given probiotic release checkpoint expectedly decreases, albeit with diminishing returns. This relationship between time to reach a given probiotic release checkpoint and release rate  $k_R$  appears to follow a negative logarithmic relationship. For the 6- and 12-hour delays, this trend does not persist because, when the delay is set to such short lengths of time, the probiotic release is subject to antibiotic interaction. As such, figures 4c and 4d are showing how antibiotic

interaction affects the time to reach probiotic release checkpoints in addition to how the release rate  $k_R$  affects this time. From figures 4c and 4d, they show that despite antibiotic interaction significantly impacting probiotic release, the release rate still causes differences between the probiotic release, and this difference becomes compounded as probiotics continue to release; hence why the 95% release checkpoints in figures 5c and 5d have more variance than the other release checkpoints.

## 4.2 Lactic Acid Release and pH Change

The initial condition of the system features a pH of 7 which is considered to be indicative of BV.

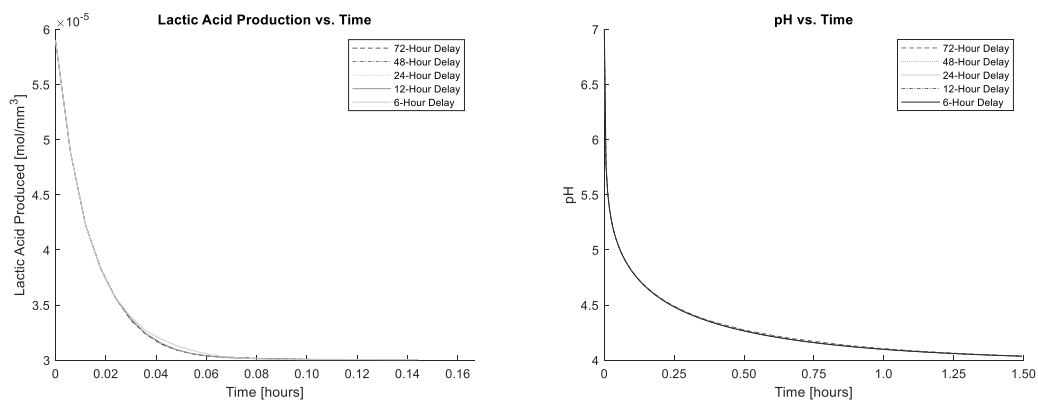


Figure 6a-b: Lactic acid release with associated pH change over time. Note that the interior of the scaffold is modeled, so lactic acid release indicates lactic acid released from the scaffold into the exterior environment. The release rate  $k_R$  was set to  $5 \times 10^{-1} \text{ h}^{-1}$ .

Elevated vaginal pH is a diagnostic indicator of BV; above 4.5 is considered elevated, a pH of 5 would be a slight infection, pH of 6 would be a moderate infection, and pH of 7 would be highly infected [7][8][4]. As a diagnostic indicator, elevated vaginal pH is not specific to BV, however it is one of the conditions in Amsel's criteria, which is the most common form of BV diagnosis [8]. A healthy vaginal pH is considered to be around pH 4

<sup>[4]</sup> so it is vital for probiotics to produce sufficient lactic acid to counteract the elevated pH and maintain a healthy environment.

Based on the modeling results, the probiotics will cause a pH shift that is sensitive to the infection level. If there is a high level of infection, the initial pH will begin at 7 and decrease to 4. However, if there is a moderate level of infection, the initial pH will begin at 6 and the probiotics cause a smaller shift in pH, resulting in the pH decreasing and reaching equilibrium at 4. With a low level of infection, a smaller shift of pH is required since the pH balance has not been disrupted as severely as with higher levels of infection. In this scenario, pH starts at 5 and decreases to equilibrium at pH 4. The modeling results indicate that regardless of initial pH, the probiotics will proliferate such that the lactic acid equilibrium yields a pH of 4. Only the initial condition of pH 7 was shown since the pH follows the same kinetics regardless of initial condition, where the lactic acid equilibrium quickly results in an equilibrium pH of roughly 4. Additionally, lactic acid release inside the scaffold as well as associated pH remain uniform across various delays since probiotics continue to produce lactic acid regardless of release status. As a result, the delay of probiotic release does not impact lactic acid production and by extension, pH. The same holds true for the impact of release rate  $k_R$  on lactic acid production and pH; since release rate only alters release of probiotic, it has no bearing on the probiotic before release occurs.

## **5. Conclusions**

The aim of this model was to simulate probiotic release patterns, pH change and assess associated recurrence prevention, release of two agents without overlap, and determine the ideal delay between probiotics and antibiotics. More broadly though, the aim was also to develop a tool that can help guide *in vitro*, *ex vivo*, or *in vivo* testing of an antibiotic-probiotic scaffold for treatment of BV and prevention of recurrent BV. The model was successful in producing probiotic release curves that avoided interaction with the antibiotic and based on the model output, a delay of at least 1 day was required, while a 2-day delay was optimal. Additionally, by modeling the effect of probiotics on pH, the probiotics showed sensitivity to varying levels of infection. With pH 7 serving as a severe infection, pH 6 serving as a moderate infection, and pH 5 serving as a slight infection, the simulated probiotics showed stronger or weaker responses based on the level of infection. At a pH indicative of infection, stronger pH shift was caused by the probiotics while a pH indicative of a weaker infection caused a smaller pH shift. More importantly, the probiotics were able to restore pH to a healthy level (pH 4) and maintain equilibrium at that pH. There still remain factors worth investigating, however. For instance, this model uses the same geometry as the fiber described in Halwes et al., however, due to the nature of 3D printing, a variety of geometries can be tested. While varying system geometry would be valuable in and of itself, perhaps more valuable would be an expansion to the model that allows for the simulation of BV infection. Currently, the model domain is restricted to a single scaffold for the sake of practicality. This means that, since *G.v.* is not loaded into scaffolds, *G.v.* are not being simulated and neither is the competition between *L.cr.* and *G.v.* Due to the lack of *G.v.* simulation, BV infection as a whole is not

being modeled; instead, only the release and proliferation of probiotics and key components related thereof. As a result, efficacy of treatment and recurrence of BV are difficult to predict from this model due to the fact that only the inside of the scaffold is simulated, and recurrence depends on conditions outside the scaffold, in the FRT.

## **6. Recommendations**

There still remain factors worth investigating, however. The first of these factors would be the characterization of drug release. The current standard for bacterial vaginosis is antibiotic treatment. Typically, metronidazole, clindamycin, or tinidazole are used for BV treatment, and the release characteristics of these antibiotics should be explored so that probiotic release can be altered accordingly. The current model uses drug diffusivity for an antiviral drug, whose release is largely based on simple diffusion. As such, it would be reasonable to extend this behavior to BV antibiotics and modifying the current model to fit these antibiotics would entail adjusting the diffusivity term in the model based on release characteristics of antibiotics from 3D-printed scaffolds. This would require experimental results that show antibiotic release from scaffolds.

Furthermore, this model uses the same geometry as the fiber described in Halwes et al.<sup>[9]</sup>, however, due to the nature of 3D printing, a variety of geometries can be tested. For instance, scaffolds can be printed in geometries resembling capsules, IVRs, etc. all with varying diameters, thicknesses, lengths, or widths. For any given geometry, a variety of dimensions can be modeled and tested.

While varying system geometry would be valuable in and of itself, perhaps more valuable would be an expansion to the model that allows for the simulation of BV infection. Currently, the model domain is restricted to a single scaffold for the sake of practicality. This means that, since *G.v.* is not loaded into scaffolds, *G.v.* are not being simulated and neither is the competition between *L.cr.* and *G.v.* Due to the lack of *G.v.* simulation, BV infection as a whole is not being modeled; instead, only the release and proliferation of probiotics and key components related thereof. As a result, efficacy of treatment and recurrence of BV are difficult to predict from this model due to the fact that only the inside of the scaffold is simulated, and recurrence depends on conditions outside the scaffold, in the FRT. Not only would infection become a possible simulation in this model, but release could be more accurately modeled. Since the model only accounts for the interior of the scaffold, the probiotic release from the scaffold into the environment is modeled, but the proliferation of probiotics after being released is not modeled. With an expansion to the model that would allow for an exterior environment to be simulated, the probiotic release can take into account proliferation after release and be more comparable to experimental data.



## References

1. CDC - Bacterial Vaginosis Statistics. (2017). Centers for Disease Control and Prevention. <https://www.cdc.gov/std/bv/STDFact-Bacterial-Vaginosis.htm>
2. Bacterial Vaginosis. (2019). Mayo Clinic.
3. Health Benefits of Taking Probiotics. (2020). Harvard Health Publishing.
4. Almassi, E. (2017). What is Bacterial Vaginosis and How do Women Get it?
5. Bouguettoucha, A., Balannec, B., & Amrane, A. (2011). Unstructured Models for Lactic Acid Fermentation - A Review. *Food Technology and Biotechnology*, 49.
6. Chen, C., Song, X., Wei, W., Zhong, H., Dai, J., Lan, Z., Li, F., Yu, X., Feng, Q., Wang, Z., Xie, H., Chen, X., Zeng, C., Wen, B., Zeng, L., Du, H., Tang, H., Xu, C., Xia, Y., Xia, H., Yang, H., Wang, J., Wang, J., Madsen, L., Brix, S., Kristiansen, K., Xu, X., Li, J., Wu, R., & Jia, H. (2017). The microbiota continuum along the female reproductive tract and its relation to uterine-related diseases. *Nat Commun*, 8(1), 875. <https://doi.org/10.1038/s41467-017-00901-0>
7. Colonna, C., & Steelman, M. (2021). Amsel Criteria. In *StatPearls*. StatPearls Publishing Copyright © 2021, StatPearls Publishing LLC.
8. Coudray, M. S., & Madhivanan, P. (2020). Bacterial vaginosis-A brief synopsis of the literature. *Eur J Obstet Gynecol Reprod Biol*, 245, 143-148. <https://doi.org/10.1016/j.ejogrb.2019.12.035>
9. Faught, B. M., & Reyes, S. (2019). Characterization and Treatment of Recurrent Bacterial Vaginosis. *J Womens Health (Larchmt)*, 28(9), 1218-1226. <https://doi.org/10.1089/jwh.2018.7383>
10. Garnier, A., & Gaillet, B. (2015). Analytical solution of Luedeking-Piret equation for a batch fermentation obeying Monod growth kinetics. *Biotechnol Bioeng*, 112(12), 2468-2474. <https://doi.org/10.1002/bit.25669>
11. Geshnizgani, A. M., & Onderdonk, A. B. (1992). Defined medium simulating genital tract secretions for growth of vaginal microflora. *J Clin Microbiol*, 30(5), 1323-1326. <https://doi.org/10.1128/jcm.30.5.1323-1326.1992>
12. Gilda, T., Muriel, A., Catronia, S. B., & Richard, A. C. (2017). The role of lactic acid production by probiotic *Lactobacillus* species in vaginal health. *Research in Microbiology*, 168(9), 782-792. <https://doi.org/https://doi.org/10.1016/j.resmic.2017.04.001>
13. Halwes, M. E., Tyo, K. M., Steinbach-Rankins, J. M., & Frieboes, H. B. (2018). Computational Modeling of Antiviral Drug Diffusion from Poly(lactic- co-glycolic-acid) Fibers and Multicompartment Pharmacokinetics for Application to the Female Reproductive Tract. *Mol Pharm*, 15(4), 1534-1547. <https://doi.org/10.1021/acs.molpharmaceut.7b01089>
14. Han, K., & Levenspiel, O. (1988). Extended monod kinetics for substrate, product, and cell inhibition. *Biotechnol Bioeng*, 32(4), 430-447. <https://doi.org/10.1002/bit.260320404>
15. Hickey, M. W., Hillier, A. J., & Jago, G. R. (1986). Transport and metabolism of lactose, glucose, and galactose in homofermentative lactobacilli. *Appl Environ Microbiol*, 51(4), 825-831. <https://doi.org/10.1128/aem.51.4.825-831.1986>

16. Krasnopolsky, V. N., Prilepskaya, V. N., Polatti, F., Zarochentseva, N. V., Bayramova, G. R., Caserini, M., & Palmieri, R. (2013). Efficacy of vitamin C vaginal tablets as prophylaxis for recurrent bacterial vaginosis: a randomised, double-blind, placebo-controlled clinical trial. *J Clin Med Res*, 5(4), 309-315. <https://doi.org/10.4021/jocmr1489w>
17. Kullen, M. J., & Klaenhammer, T. R. (1999). Identification of the pH-inducible, proton-translocating F1F0-ATPase (atpBEFHAGDC) operon of *Lactobacillus acidophilus* by differential display: gene structure, cloning and characterization. *Mol Microbiol*, 33(6), 1152-1161. <https://doi.org/10.1046/j.1365-2958.1999.01557.x>
18. Liu, Y., Tran, D. Q., & Rhoads, J. M. (2018). Probiotics in Disease Prevention and Treatment. *J Clin Pharmacol*, 58 Suppl 10(Suppl 10), S164-s179. <https://doi.org/10.1002/jcph.1121>
19. Luedeking, R., & Piret, E. L. (2000). A kinetic study of the lactic acid fermentation. Batch process at controlled pH. Reprinted from *Journal of Biochemical and Microbiological Technology Engineering* Vol. I, No. 4. Pages 393-412 (1959). *Biotechnol Bioeng*, 67(6), 636-644. [https://doi.org/10.1002/\(sici\)1097-0290\(20000320\)67:6<636::aid-bit3>3.0.co;2-u](https://doi.org/10.1002/(sici)1097-0290(20000320)67:6<636::aid-bit3>3.0.co;2-u)
20. Lykke, M. R., Becher, N., Haahr, T., Boedtkjer, E., Jensen, J. S., & Uldbjerg, N. (2021). Vaginal, Cervical and Uterine pH in Women with Normal and Abnormal Vaginal Microbiota. *Pathogens*, 10(2). <https://doi.org/10.3390/pathogens10020090>
21. Monod, J. (1949). THE GROWTH OF BACTERIAL CULTURES. *Annual Review of Microbiology*, 3(1), 371-394. <https://doi.org/10.1146/annurev.mi.03.100149.002103>
22. Tyo, K. M., Minooei, F., Curry, K. C., NeCamp, S. M., Graves, D. L., Fried, J. R., & Steinbach-Rankins, J. M. (2019). Relating Advanced Electrospun Fiber Architectures to the Temporal Release of Active Agents to Meet the Needs of Next-Generation Intravaginal Delivery Applications. *Pharmaceutics*, 11(4). <https://doi.org/10.3390/pharmaceutics11040160>
23. National Center for Biotechnology Information (2021). PubChem Compound Summary for CID 612, Lactic acid. Retrieved November 11, 2021 from <https://pubchem.ncbi.nlm.nih.gov/compound/Lactic-acid>.
24. Colucci Cante, R., et al., Mathematical Modeling of *Lactobacillus paracasei* CBA L74 Growth during Rice Flour Fermentation Performed with and without pH Control. *Applied Sciences*, 2021. 11(7): p. 2921.
25. Chawla, D., et al., *3D bioprinted alginate-gelatin based scaffolds for soft tissue engineering*. *Int J Biol Macromol*, 2020. **144**: p. 560-567.
26. You, F., et al., 3D Printing of Porous Cell-Laden Hydrogel Constructs for Potential Applications in Cartilage Tissue Engineering. *ACS Biomater Sci Eng*, 2016. 2(7): p. 1200-1210.
27. Clark, J.T., et al., Quantitative evaluation of a hydrophilic matrix intravaginal ring for the sustained delivery of tenofovir. *J Control Release*, 2012. 163(2): p. 240-8.
28. Briggs, G.E. and J.B. Haldane, A Note on the Kinetics of Enzyme Action. *Biochem J*, 1925. 19(2): p. 338-9.

29. Michaelis, L., et al., The original Michaelis constant: translation of the 1913 Michaelis-Menten paper. *Biochemistry*, 2011. 50(39): p. 8264-9.
30. Bernardo, M.P., et al., l-(+)-Lactic acid production by *Lactobacillus rhamnosus* B103 from dairy industry waste. *Braz J Microbiol*, 2016. 47(3): p. 640-6.
31. Komesu, A., et al., Lactic Acid Production to Purification: A Review. *BioResources*, 2017. 12: p. 4364 - 4383.
32. Tietz, K., & Klein, S. (2018). Simulated Genital Tract Fluids and Their Applicability in Drug Release/Dissolution Testing of Vaginal Dosage Forms. *Dissolution Technologies*, 25(3), 40+.
33. Cohen, C.R., et al., *Randomized Trial of Lactin-V to Prevent Recurrence of Bacterial Vaginosis*. *N Engl J Med*, 2020. **382**(20): p. 1906-1915.
34. Homayouni, A., et al., Effects of probiotics on the recurrence of bacterial vaginosis: a review. *J Low Genit Tract Dis*, 2014. 18(1): p. 79-86.
35. Januszewicz, R., et al., Design and Characterization of a Novel Series of Geometrically Complex Intravaginal Rings with Digital Light Synthesis. *Adv Mater Technol*, 2020. 5(8).
36. Display Format for Numeric Values - MATLAB & Simulink. Format [cited 2021 12/01]; Available from: [https://www.mathworks.com/help/matlab/matlab\\_prog/display-format-for-numeric-values.html](https://www.mathworks.com/help/matlab/matlab_prog/display-format-for-numeric-values.html).
37. Double-precision arrays - MATLAB. X [cited 2021 12/01]; Available from: <https://www.mathworks.com/help/matlab/ref/double.html>.
38. Oppenheimer, D. Understanding floating point precision, aka "Why does excel give me seemingly wrong answers?". Microsoft 365 Blog [cited 2021 12/01]; Available from: <https://www.microsoft.com/en-us/microsoft-365/blog/2008/04/10/understanding-floating-point-precision-aka-why-does-excel-give-me-seemingly-wrong-answers/>.